Shock-induced behavior of cubic gauche polymeric nitrogen

William D. Mattson and Radhakrishnan Balu
U.S. Army Research Laboratory, RDRL-WML-B (Bldg. 4600), Aberdeen Proving Ground, Maryland 21005-5069, USA
(Received 26 January 2011; revised manuscript received 8 April 2011; published 11 May 2011)

Quantum-mechanical calculations based on density functional theory are used to study the shock response of the polymeric cubic gauche phase of nitrogen (cg-N), proposed as an alternative energetic ingredient to those used in conventional explosive formulations. The shocked polymeric nitrogen undergoes multiple complex phase transformations and spontaneously forms defects. The occurrence of these dynamic phenomena absorbs the shock energy which subsequently slows the compression wave. Additionally, no reaction occurs immediately behind the shock front; rather reactions result from the unraveling of the material at the free edge of the filament opposite to shock propagation. As the material unravels, numerous polyatomic transients are formed, including five-membered rings and polymeric chains, which subsequently undergo secondary reactions to form the final diatomic products. The speed at which these reactions propagate through the material is much slower than the sound speed, and combined with the slowing compression wave, indicates that the material may not detonate under these conditions.

DOI: 10.1103/PhysRevB.83.174105 PACS number(s): 62.50.Ef, 82.40.Fp, 61.50.Ah, 61.72.Cc

I. INTRODUCTION

Pressure-induced transitions of molecular solids to polymeric forms have been the subject of intense activity for several decades. One of the more widely studied systems both theoretically[1–24] and experimentally[25–40] is nitrogen, which in its ambient state is a homonuclear diatomic molecule with one of the strongest bonds in nature, making it an ideal candidate for energy storage if a stable high-density polymeric form can be realized. Theoretical predictions have indicated a variety of possible molecular and polymeric phases over a range of pressures and temperatures; however, until recently, only the diatomic molecular high-pressure phases were observed experimentally within the predicted pressure and temperature regimes. Phase transitions to the more exotic polymeric[31,33,34] and nondiatomic molecular phases[36] have been observed well above the predicted transition pressure range for the diatomic to cubic gauche (cg-N) transition.[5] This cg-N form of nitrogen is a bulk three-dimensional covalent network, similar to diamond, in which every atom has three neighbors. This structure was observed in diamond-anvil-cell experiments[39] in which nitrogen is compressed to 180 GPa and heated to 2200 K. The sample was only partially cg-N and included amorphous polymeric nitrogen. The material was not recoverable at ambient conditions, although phonon calculations indicate that the cg-N structure should be stable at ambient pressures.[41] However, all theoretical calculations have assumed an ideal crystal structure, which is not attainable under the extreme experimental conditions used in its synthesis, and thus the presence of these other phases most likely introduces instabilities preventing the recovery of the cg-N at ambient conditions. Continued theoretical and experimental explorations to understand the principle physical and chemical laws which govern bonding, phase behavior, and thermodynamic stability of high-pressure polymeric phases are necessary for developing the technologies required to recover polymeric forms of nitrogen at the ambient state.

These new types of materials are not only of academic interest, as the large energy densities of some of the various polymeric forms make them promising high-performing alternatives to currently fielded conventional energetic materials (EM). The calculated energy of complete conversion of cg-N to the ground state diatomic nitrogen ranges from 0.75 to 1.55 eV per atom,[12] several times that of conventional explosives.[42] However, before cg-N can be considered for use in a practical EM application, its stability and dynamic response under a variety of conditions must be well understood. This study is the first in a series in which such factors are explored, where we present quantum molecular-dynamics (QMD) results of shocked cg-N initially at low temperature and ambient pressure.

Finally, one of the primary goals of this paper is to determine whether shock impact will initiate a self-sustained reaction wave within the defect-free cg-N material. In addition to presenting results demonstrating the dynamic response of shocked cg-N, this paper will briefly describe the theoretical methods, the computational details, software explored to enable adequate treatment of the calculations, and results of the calculations to date.

II. DETAILS OF THE CALCUATION

The first-principles calculations reported herein use the Kohn-Sham density functional theory (DFT) with the generalized gradient approximation (GGA) exchange-correlation functional of Perdew, Burke, and Ernzerhof (PBE).[43] QMD simulations were performed using the Gaussian and plane-wave-method code QUICKSTEP as implemented in CP2K (Ref. 44) and the double-zeta with valence polarization basis. Total energies and forces were converged to 2.6×10^{-5} and 1.6×10^{-4} a.u., respectively, for all calculations. The equations of motion are from the Born-Oppenheimer approximation with a time step of 1 fs for all simulations.

The direct shock-wave simulations here are implemented with a long thin filament[45] composed of blocks of eight-atom simple cubic cells. Each block is constructed using two instances of the primitive cell of cg-N (space group $I2_13$5) with one centered at the origin (0,0,0) and the other at the body-centered site (1/2,1/2,1/2). The blocks are used to create

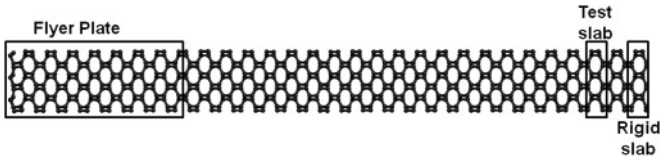

FIG. 1. A schematic of the filament used in the QMD simulations of shock-impacted cg-N. The filament can be described as a series of blocks composed of (1 × 3 × 3) unit cells of cg-N. The block at the far right edge of the filament (outlined in black) denotes the material that is fixed during the simulation; to its left is the "test" block, used to determine shock-wave approach (see text). The eight blocks at the far left edge of filament contain the flyer plate atoms.

a "slab" which is defined to be a (1 × 3 × 3) supercell of blocks with dimensions of (3.8,11.3,11.3) Å. The filament is then composed of 32 slabs of cg-N. The simulation cell, shown in Fig. 1, contains 2304 atoms. In order to generate an initial configuration for use in the shock simulation, the 0 K configuration was first obtained through geometry optimization of the filament. Next, the optimized simulation cell was first subjected to an isothermal isochoric (NVT) MD simulation at either $T = 200$ or 300 K for 5 ps. The final configuration of the NVT-MD simulation was then used in an isothermal-isobaric (NPT) MD simulation at either $T = 200$ or 300 K, $P = 1$ bar for 5 ps to produce the filaments that would be used in the shock simulations. In all of the aforementioned simulations, periodic boundary conditions were imposed in all directions.

For the shock-wave simulations, computational schemes for reducing the costs of MD simulations of shocked crystals were employed; specifically, that outlined by Rice.[46] In this scheme, a shock wave is initiated in the filament composed of quiescent material [denoted as cg-N(V) and shown in Fig. 1] through flyer plate impact. Periodic boundary conditions are imposed in the two directions perpendicular to the direction of the shock impact and propagation (in this case, the x direction). For these simulations, the shock will be introduced at the far-left side of the filament by a "flyer plate" composed of cg-N. These correspond to the eight leftmost slabs shown in Fig. 1. The edge of the simulation cell opposite to shock impact is bounded by a slab of constrained atoms (located at the right edge of Fig. 1). Within this scheme, as the shock wave approaches the rigid layer, additional undisturbed material is inserted before the rigid layer to allow continuance of the shock wave. The shock wave can be initiated through instantaneously increasing the x component of the velocity of each atom within the flyer plate by an additional 10 km/s. Following Rice *et al.*, a (1 × 3 × 3) test slab was monitored for shock-wave approach and is located one slab length to the left of the rigid slab of atoms in the filament (see Fig. 1). The center-of-mass displacement within the "test slab" is evaluated at each integration step and when this value exceeded that of thermally equilibrated bulk cg-N by 0.1 Å, material composed of thermally equilibrated bulk cg-N is inserted between the rightmost slab of moving atoms and the rigid layer. The filament has a "free edge" at the leftmost region (the flyer plate) with vacuum to the left. We confirmed that the material with the free edge was stable at both $T =$ 200 or 300 K using NVT-MD simulations integrated for 15 ps. In these simulations, the initial configuration of the free-edge filament was that of the final configuration of the heretofore described NPT-MD simulation in which periodic boundary conditions were imposed in all three dimensions. During these NVT-MD simulations the atoms at the free edge exhibited larger oscillations about their lattice sites than those in the interior of the filament; however, no reaction was observed. Also, relaxation of the atoms near the free surface occurred, resulting in a slight decrease in lattice spacing relative to that within the interior of the filament.

A potential source of error is the small cross-sectional area (11.3 × 11.3 Å) normal to the direction of the shock front. However, previous quantum molecular- dynamics shock simulations have successfully used cells with similarly sized cross-sectional areas.[47,48] These calculations were performed in conjunction with the multiscale shock technique (MSST) for systems of either 64 water molecules or 360 carbon atoms. In both studies, exploration of the effect of system size showed that the simulation cells were sufficiently large to reach converged results. Also, QMD calculations of the shock Hugoniot of nitrogen over a large range of temperatures and densities using systems composed of 32, 54, and 64 atoms showed that of the measured properties, only the Gruneisen parameter showed a dependence on size, and only for the region of the shock Hugoniot where the smaller system predicted a negative value.[49] Since our simulations have substantially larger cross-sectional areas than in Ref. 49, we do not expect the results to be affected by our choice of system size.

Another potential source of error is that these simulations were performed using Born-Oppenheimer QMD and therefore the electrons in the system are treated adiabatically. Shock simulations on deuterium[50] and water[47] has shown that treating the electrons nonadiabatically within Car-Parrinello QMD (CPMD) had little effect on simulations with shock velocities less than 15 and 12 km/s, respectively. Since the electron-ion coupling constant for nitrogen is smaller than that for deuterium and hydrogen, it is expected that shock simulations of nitrogen will be insensitive to the nonadiabatic deviations of CPMD at the shock velocity investigated in this study (10 km/s). While the nonadiabatic excitation reflected by CPMD might not adequately represent that in a shock event, the insensitivity of the simulations to CPMD excitations for shock velocities of 10 km/s implies that the Born-Oppenheimer approximation is reasonable for the simulations presented here. The shock velocity for the simulation was chosen to impart sufficient energy that might lead to reaction, but was not likely to induce nonadiabatic effects.

To illustrate the evolution of the material under shock, temporal profiles of various properties within the filament will be described; this is accomplished by taking a weighted moving average of the properties in local regions of the material along the direction of the shock. For each plane normal to the x xis on intervals of 0.5 Å, the weighted moving average is calculated by summing the weighted value of the property of each atom within 4 Å of the plane under consideration. The weight assigned for each atom is proportional to its distance from the plane. For example, at 4 Å the weight is 0, and at 0 Å from the plane the weight is 0.25. This scheme produces temporally averaged values that make the relevant aspects of the simulation clear, and maintains correspondence

of the property depicted in the temporal profiles to that of the material property. Finally, in this work, chemical bonds are depicted between atom pairs with interatomic separations that are less than 1.6 Å. This value was selected after observing the temporal behavior of such bonds in the shocked lattice and in various vibrationally hot product species.

III. RESULTS

The shock-wave simulations for filaments at 200 and 300 K were performed within the microcanonical ensemble (NVE-MD) using the final configurations and atomic velocities from the NVT-MD simulations of the free-edge filament (with flyer plate atoms given the appropriate impact velocity as described heretofore). As the shock wave propagated through the material, its effects reached the test slab after 480 fs, at which time the simulations were stopped. The features of the shocked material were similar for both 200 and 300 K filaments up to this time, including phase transitions and spontaneous formation of defects, as will be discussed hereafter. Thus, further investigation is limited to the 300 K filament. For the 300 K filament simulation, an additional 25 slabs (containing 1800 atoms) were inserted immediately to the left of the rightmost rigid slab to allow the continuation of the shock simulation, increasing the total number of atoms in the filament to 4104. As shown in earlier classical molecular-dynamics studies of shocked filaments, such a scheme allows for simulation of only the area of immediate interest (i.e., the shocked region), with the idea that simulating infinitely large material well ahead of the shock discontinuity provides no extra information on the shock phenomena.[46] All results discussed hereafter refer to the simulation using the 300 K filament.

A. Complex phase transitions and defects

A series of snapshots of atomic positions at various times during the simulation (Fig. 2) illustrates the very complex behavior of shocked cg-N, with the formation of numerous phases as well as interesting reaction intermediates displayed. Figure 2(a) shows that the original honeycomb structure of the cg-N collapses to a herringbonelike lattice as the flyer plate drives the material forward. This phase [denoted HB(l)] continues to grow as the simulation progresses to a maximum width of ∼50 Å and propagates through the material in the direction of the initial shock at a gradually diminishing velocity as will be discussed in greater detail in Sec. III C. In this phase transition, no bonds are broken or formed. At 400 fs [Fig. 2(c)] additional complexity in the form of a region of compressed cg-N behind the leading phonon but ahead of the HB(l) phase emerges. This region will be denoted hereafter as the leading compression zone (LCZ). The LCZ continues to develop behind the shock front for the remainder of the trajectory. Also in Fig. 2(c), the appearance of a spontaneously formed stacking fault is apparent between the HB(l) phase (denoted as D_1 and enclosed by a box) and the LCZ. In Fig. 2(d), the material immediately to the right of D_1 deforms to a HB lattice configuration that corresponds to a shifting of the HB(l) crystal along the vertical axis by half of the original lattice vector [denoted hereafter as HB(r)]. The formation of this stacking fault was unexpected and has significant consequences, as will be discussed below. Finally, as the HB(l) phase relaxes and expands on the left, the material reforms to the cg-N structure. Note that the reformed cg-N phase has a different crystalline orientation than the initial structure. The undisturbed crystal ahead of the leading phonon has the long axis of the large honeycomblike rings oriented vertically, but the reformed region in Fig. 2(f) has the long axis of the rings oriented horizontally. Therefore, the material in the reformed cg-N phase will be denoted as cg-N(H) hereafter, whereas the material ahead of the shock front will be denoted as cg-N(V). The nearest neighbors of the nitrogen atoms in the cg-N(H) region are the same as that of cg-N(V), as is the handedness of the crystal.

More complex structures evolve in this shocked material as the trajectory continues. Specifically, at 690 fs, a new "defect"

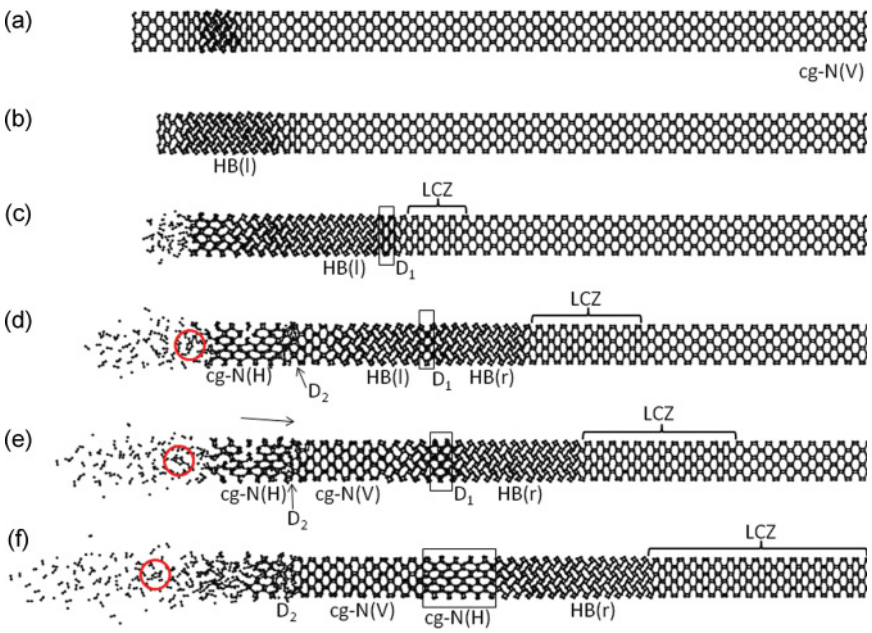

FIG. 2. (Color online) Snapshots of the cg-N system at (a) $t = 90$ s, (b) 160 fs, (c) 400 fs, (d) 690 fs, (e) 830 fs, and (f)1040 fs. For clarity, the block of stationary atoms at the far-right edge of the simulation cell are not shown; also, quiescent crystal is added to the snapshots in (a)–(c) to have the same x dimension as those in (d)–(f). See text for explanation of the larger simulation cells used in (d)–(f).

appears (denoted D_2), which is bounded by the cg-N(H) structure on the left and a reformed cg-N(V) on the right. To the right of these are the HB phases (which also have in their midst D_1, discussed above) and the LCZ. In D_2, bonds are broken and formed, unlike the material associated with D_1. At 830 fs [Fig. 2(e)], D_1 has widened and by 1040 fs has transitioned into the cg-N(H) phase [see the region enclosed by the box in Fig. 2(f)]. The width of the HB(l) phase decreases during the transition of D_1 to the cg-N(H) phase, a result both from back transition to cg-N(V) at its left boundary and from back transition of D_1 to cg-N(H) at its right boundary. The HB(r) phase to the right of D_1 is maintained as the LCZ transitions to HB(r); the LCZ material to its right continues to widen.

B. Chemical reaction

Reactions in the shocked material are equally complex and interesting. Initially, as seen in the snapshot at 400 fs [Fig. 2(c)], most of the products ejected from the free cg-N surface at the left are diatomic nitrogen, with a few short-lived N_3 molecules. As soon as two N_3 molecules approach each other, they rapidly react to form three N_2 molecules. By 690 fs [Fig. 2(d)], chains with one end connected to the leftmost free surface start to form, break free at the surface, and subsequently decompose. As chains continue to form, their lengths increase and disintegration occurs within the chains rather than detachment at the surface. The lengthening of these chains indicates that surface disintegration of the cg-N lattice occurs more quickly than formation of the more stable N_2 product. By 1040 fs [Fig. 2(f)], large fragments of crystal have disintegrated into chains. This process creates a reaction zone with little to no N_2 forming at the cg-N surface, but rather N_2 resulting from reactions of the detached chains. Additionally, other more complicated structures are formed including N_5 rings [see, for example, the ring in Figs. 2(d)–2(f) bounded by the red circle]. Some of the N_5 rings also have chains attached to one of the atoms in the ring. Figure 3 shows a time history of the formation and progression of the N_5 ring highlighted in the snapshots in Fig. 2. This five-membered ring within the red circle has a lifetime of in excess of 450 fs as evidenced by the temporal history of the bonds labeled on the moiety shown in Fig. 4. Up to 770 fs, the pentazole ring has a six-membered nitrogen chain attached to it at which point the nitrogen chain subsequently decomposes into three nitrogen molecules. The chain decomposes first by simultaneously forming two nitrogen molecules from the four terminal nitrogen atoms of the chain, followed by the dissociation of the remaining two nitrogen atoms from the pentazole ring to form the final nitrogen molecule. By 820 fs, the three nitrogen molecules oscillate about the equilibrium gas phase value (1.1 Å), while the bonds corresponding to the pentazole ring oscillate about larger values (∼1.3–1.4 Å) for the remainder of the trajectory integration. Pentazole structures have been shown to be stable[51] and similar structures have recently been observed in simulations calculating the high-temperature phase diagram of nitrogen.[52,53] Interestingly, both Boates *et al.*[52] and Donadio *et al.*[53] have observed a liquid-liquid phase transition where the liquid molecular nitrogen transforms into nitrogen chains and five-membered rings, similar to the reaction intermediates shown in the simulations herein.

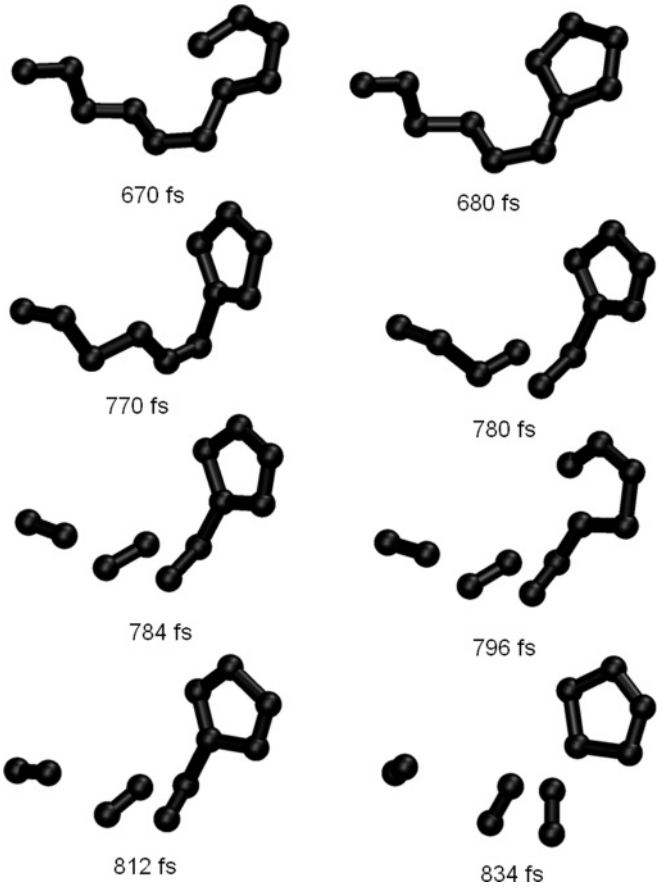

FIG. 3. Snapshots of one of the longer-lived polyatomic transients formed in the reaction zone of the material. Times during the simulation are denoted in the figure.

C. Spatial-temporal profiles of material properties

Spatial-temporal profiles of the velocity of particles of the material in the supercell along the direction of shock propagation are given in Fig. 5. In the figure the length of the supercell in the direction of shock propagation corresponds to the x axis and the simulation time corresponds to the y axis. The red triangular region in the lower left-hand area of the figure corresponds to the initial flyer plate. Partitions corresponding to a portion of the vacuum region to the left of the initial flyer plate position and corresponding to the fixed slab (far right of the simulation cell) are not shown. The phonons emanating in front of the shock discontinuity are clearly apparent in Fig. 5, with an initial phonon generated by the shock impact (∼150 fs) and progressing ahead of a series of evolving shock fronts. We define a shock front as a nearly discontinuous change in material state during the simulation. Additionally, density profiles along the filament at later times indicate a series of subsequent phonons emanating ahead of the leading shock front. By the end of the simulation, five very distinct phonons have appeared and are traveling at a constant speed of 16.5 ±0.5 km/s. The compressed region behind the phonons, however, is clearly slowing down. At the initial stages of its formation, the velocity of the leading edge of the HB(l) phase aligns with the initial phonon. Interestingly, at 40 Å, ∼150 fs, a second phonon emanates, with an almost discontinuous decrease in velocity of the shock front. A similar

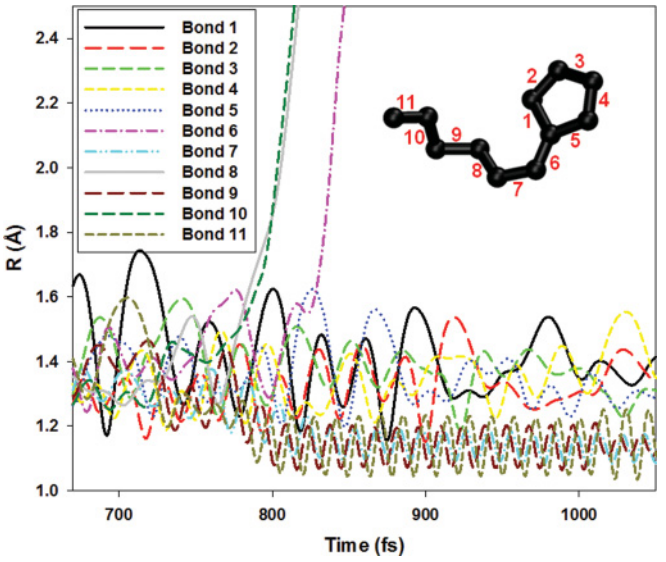

FIG. 4. (Color online) Time trace of the bond lengths of the bonds shown in Fig. 3. The bonds are numbered in the inset moiety which is a copy of the 680 fs snapshot in Fig. 3.

manifestation of this behavior is apparent at 90 Å, 550 fs, in which a third phonon appears with a corresponding decrease in velocity of the shock front. Beyond that, two additional phonons appear and the shock front continues to slow.

Figure 6 shows the instantaneous temperature profile of the material in the supercell along the direction of shock propagation. The local temperatures within the material were calculated by first subtracting the weighted center-of-mass velocity of all atoms in the local region around each plane from the individual atomic velocities in the local region, and then used to calculate an instantaneous local temperature. There is significant heterogeneity within the material phases as shown in Fig. 6. Of most importance is the region where the initial spontaneously formed stacking fault (D_1) resides. It is notable that the temperature of the area around the fault remains lower than the material on either side of it. The stacking fault, which first appears at ~400 fs, corresponds to the point in Fig. 6 at

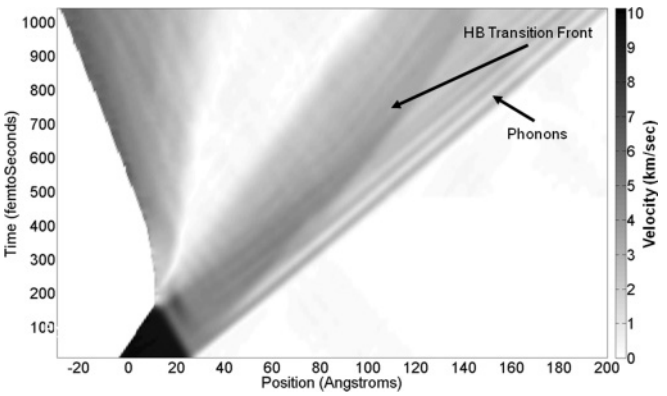

FIG. 5. Temporal velocity profiles. Phonons emanate from the shock front and propagate at a velocity of 16.5 km/s away from the shock front. The shock front (HB transition front) itself slows down. Legends for the color range are given in the figure for the range of 0 to 10.1 km/s.

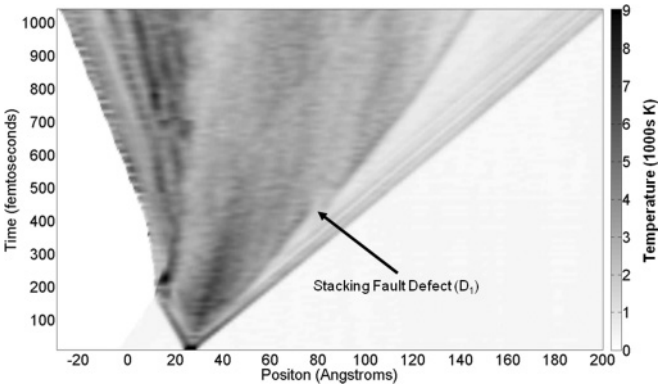

FIG. 6. Temporal instantaneous temperature profiles. The temperature of the defect is lower than the surrounding compressed region. Legends for the color range are given in the figure for the range of 0 to 9000 K.

which the velocities of the second phonon, and the following compressed region, separate. The region corresponding to D_1 remains lower in temperature than the material ahead or behind it all throughout the simulation, indicating that the stacking fault acts as an energy sink.

IV. DISCUSSION

It was expected that cg-N, like all other forms of polymeric nitrogen, would be an advanced, new type of energetic material due to its stored structural energy. The transition to gaseous nitrogen would release 1.55 eV/atom,[12] a substantially higher energy release than that of conventional energetic materials. Unfortunately, the results of these simulations indicate that the mechanical properties of cg-N in its purest, defect-free, form enable it to disperse shock energy through extremely complex phase transitions such that initiation to a self-sustained exothermic shock-driven reaction is improbable. Most likely, the reaction within the rarefaction region could continue until the material is consumed but at a rate that would preclude cg-N from consideration as an advanced high explosive.

It is worth noting at this point that Chen *et al.*[19] performed first-principles calculations of mechanical properties and failure modes for cg-N, and concluded that this material has "exceptional mechanical properties." They evaluated the failure modes for cg-N using the method of Roundy *et al.*[54] in which the lattice vectors are incrementally deformed in the direction of the applied stress and the atomic coordinates are fully relaxed between increments. In this study they found that the dominant mode of lattice failure is shear, a condition not imposed in the shock simulations contained in this effort. The size of the simulation cell used in this study is too small to allow the formation of shock-induced shear bands and therefore, the role of shear on dynamic response cannot be evaluated using these results.

An equally important consideration is the role of defects on the shock response of cg-N. Synthesized cg-N will include defects, which could influence the shock behavior, as evidenced by the role spontaneously formed defects play in the dynamic response of the pure material discussed above. Although it is well beyond the scope of the current study, a thorough QMD investigation of a shocked defected material could identify

fundamental mechanisms that contribute to the physical response of the material, including plasticity, fragmentation, defect-nucleated reactions, and melting. In light of the possible roles of shear and/or defects in the shocked material on reactivity and energy release, it would be premature to conclude that cg-N would not be useful as an energetic material.

V. SUMMARY

Quantum MD simulations have been used to provide an atomic-level description of the material response of the defect-free cg-N polymeric form of solid nitrogen to shock. The cg-N solid showed extremely complex shock-wave structure involving several structural phase changes and spontaneous formation of material defects behind the shock front that absorbed and dispersed the shock energy. Reaction did not occur directly behind the shock front, but rather at the free edge of the filament opposite to the direction of shock propagation, unraveling into a variety of polyatomic and polymeric transients, including chains and five-member rings. These transients subsequently decomposed or underwent collision with other transients to form the final diatomic product gas. The heat released in the reactions was localized in this dense-gas region behind the disintegrating filament and not transferred to the remaining intact filament. Although the simulations suggest that the pure form of cg-N might not be a good candidate for use as an explosive, its unique energy dispersion properties due to the complex phase transitions initiated by shock could be exploited for other applications in which such a response would be advantageous.

ACKNOWLEDGMENTS

Calculations were performed using the DOD Supercomputing Resource Centers (DSRCs) located at the U.S. Army Research Laboratory and the Air Force Research Laboratory under the Computing Challenge Project C2L awarded by the DOD High Performance Computing Modernization Program. R.B. acknowledges support from the Research Participation Program for the U.S. Army Research Laboratory administered by the Oak Ridge Institute for Science and Education. The authors wish to thank Betsy Rice for helpful comments and discussions.

[1] R. LeSar, J. Chem. Phys. **81**, 5104 (1984).
[2] A. K. McMahan and R. LeSar, Phys. Rev. Lett. **54**, 1929 (1985).
[3] R. M. Martin and R. J. Needs, Phys. Rev. B **34**, 5082 (1986).
[4] S. P. Lewis and M. L. Cohen, Phys. Rev. B **46**, 11117 (1992).
[5] C. Mailhiot, L. H. Yang, and A. K. McMahan, Phys. Rev. B **46**, 14419 (1992).
[6] L. Mitas and R. M. Martin, Phys. Rev. Lett. **72**, 2438 (1994).
[7] M. M. G. Alemany and J. L. Martins, Phys. Rev. B **68**, 024110 (2003).
[8] L. N. Yakub, Low. Temp. Phys. **29**, 780 (2003).
[9] W. D. Mattson, D. Sanchez-Portal, S. Chiesa, and R. M. Martin, Phys. Rev. Lett. **93**, 125501 (2004).
[10] F. Zahariev, A. Hu, J. Hooper, F. Zhang, and T. Woo, Phys. Rev. B **72**, 214108 (2005).
[11] H. L. Yu, G. W. Yang, X. H. Yan, Y. Xiao, Y. L. Mao, Y. R. Yang, and M. X. Cheng, Phys. Rev. B **73**, 012101 (2006).
[12] J. Uddin, V. Barone, and G. E. Scuseria, Mol. Phys. **104**, 745 (2006).
[13] T. Zhang, S. Zhang, Q. Chen, and L.-M. Peng, Phys. Rev. B **73**, 094105 (2006).
[14] F. Zahariev, S. V. Dudiy, J. Hooper, F. Zhang, and T. K. Woo, Phys. Rev. Lett. **97**, 155503 (2006).
[15] A. R. Oganov and C. W. Glass, J. Chem. Phys. **124**, 244704 (2006).
[16] F. Zahariev, J. Hooper, S. Alavi, F. Zhang, and T. K. Woo, Phys. Rev. B **75**, 140101 (2007).
[17] R. Caracas and R. J. Hemley, Chem. Phys. Lett. **442**, 65 (2007).
[18] X. L. Wang, X. He, Y. M. Ma, T. Cui, Z. M. Liu, B. B. Liu, J. F. Li, and G. T. Zou, J. Phys.: Condens. Matter **19**, 425226 (2007).
[19] X. Q. Chen, C. L. Fu, and R. Podloucky, Phys. Rev. B **77**, 064103 (2008).
[20] Y. Yao, J. S. Tse, and K. Tanaka, Phys. Rev. B **77**, 052103 (2008).
[21] H. Katzke and P. Toledano, Phys. Rev. B **78**, 064103 (2008).
[22] J. Kotakoski and K. Albe, Phys. Rev. B **77**, 144109 (2008).
[23] Y. Ma, A. R. Oganov, Z. Li, Y. Xie, and J. Kotakoski, Phys. Rev. Lett, **102**, 065501 (2009).
[24] X. Wang, F. Tian, L. Wang, T. Cui, B. Liu, and G. Zou, J. Chem. Phys. **132**, 024502 (2010).
[25] A. F. Schuch and R. L. Mills, J. Chem. Phys. **52**, 6000 (1970).
[26] R. Reichlin, D. Schiferl, S. Martin, C. Vanderborgh, and R. L. Mills, Phys. Rev. Lett. **55**, 1464 (1985).
[27] R. L. Mills, B. Olinger, and D. T. Cromer, J. Chem. Phys. **84**, 2837 (1986).
[28] P. M. Bell, H. K. Mao, and R. J. Hemley, Physica B & C **139-140**, 16 (1986).
[29] R. Bini, M. Jordan, L. Ulivi, and H. J. Jodl, J. Chem. Phys. **108**, 6849 (1998).
[30] H. Olijnyk and A. P. Jephcoat, Phys. Rev. Lett. **83**, 332 (1999).
[31] A. F. Goncharov, E. A. Gregoryanz, H. K. Mao, Z. Liu, and R. J. Hemley, Phys. Rev. Lett. **85**, 1262 (2000).
[32] R. Bini, L. Ulivi, J. Kreutz, and H. J. Jodl, J. Chem. Phys. **112**, 8522 (2000).
[33] M. I. Eremets, R. J. Hemley, H. K. Mao, and E. Gregoryanz, Nature (London) **411**, 170 (2001).
[34] E. Gregoryanz, A. F. Goncharov, R. J. Hemley, and H. K. Mao, Phys. Rev. B **64**, 52103 (2001).
[35] A. F. Goncharov, E. Gregoryanz, H.-K. Mao, and R.J. Hemley, Low Temp. Phys. **27**, 866 (2001).
[36] E. Gregoryanz, A. F. Goncharov, R. J. Hemley, and H. K. Mao, Phys. Rev. B **66**, 224108 (2002).
[37] M. I. Eremets, A. G. Gavriliuk, I. A. Trojan, D. A. Dzivenko, and R. Boehler, Nat. Mater. **3**, 558 (2004).
[38] M. I. Eremets, A. G. Gavriliuk, N. R. Serebryanaya, I. A. Trojan, D. A. Dzivenko, R. Boehler, H. K. Mao, and R. J. Hemley, J. Chem. Phys. **121**, 11296 (2004).
[39] E. Gregoryanz, A. F. Goncharov, C. Sonloup, M. Somayazulu, H. Mao, and R. J. Hemley, J. Chem. Phys. **126**, 184505 (2007).
[40] M. I. Eremets, A. G. Gavriliuk, and I. A. Trojan, Appl. Phys. Lett. **90**, 171904 (2007).
[41] T. W. Barbee III, Phys. Rev. B **48**, 9327 (1993).

[42]C. J. Wu and L. E. Fried, J. Phys. Chem. A **101**, 8675 (1997).
[43]J. P. Perdew, K. Burke, and M. Ernzerhof, Phys. Rev. Lett. **77**, 3865 (1996).
[44]J. VandeVondele, M. Krack, F. Mohamed, M. Parrinello, T. Chassaing, and J. Hutter, Comput. Phys. Commun. **167**, 103 (2005).
[45]B. M. Rice, W. Mattson, and S. F. Trevino, Phys. Rev. E **57**, 5106, (1998); B. M. Rice, W. Mattson, J. Grosh, and S. F. Trevino, **53**, 611 (1996); **53**, 623, (1996).
[46]B. M. Rice, *Molecular Simulation of Detonation, in Modern Methods for Multidimensional Dynamics Computations in Chemistry*, edited by D. L. Thompson (World Scientific Press, New Jersey, 1998).
[47]N. Goldman, E. J. Reed, I.-F. W. Kuo, L. E. Fried, C. J. Mundy, and A. Curioni, J. Chem. Phys. **130**, 124517 (2009).
[48]C. J. Mundy, A. Curioni, N. Goldman, I.-F. W. Kuo, E. J. Reed, L. E. Fried, and M. Ianuzzi, J. Chem. Phys. **128**, 184701 (2008).
[49]J. D. Kress, S. Mazevet, L. A. Collins, and W. W. Wood, Phys. Rev. B **63**, 024203 (2000); S. Mazevet, J. D. Johnson, J. D. Kress, L. A. Collins, and P. Blottiau, **65**, 014204 (2001).
[50]F. Gygi and G. Galli, Phys. Rev. B **65**, 220102 (2002).
[51]M. Noyman, S. Zilberg, and Y. Haas, J. Phys. Chem. A **113**, 7376 (2009).
[52]B. Boates and S. A. Bonev, Phys. Rev. Lett. **102**, 015701 (2009).
[53]D. Donadio, L. Spanu, I. Duchemin, F. Gygi, and G. Galli, Phys. Rev. B **82**, 020102 (2010).
[54]D. Roundy, C. R. Krenn, M. L. Cohen, and J. W. Morris Jr., Phys. Rev. Lett. **82**, 2713 (1999).